Acta Crystallographica Section D
Biological Crystallography
ISSN 0907-4449

Distinguishing between Cl^- and O_2^{2-} as the bridging element between Fe^{3+} and Cu^{2+} in resting-oxidized cytochrome *c* oxidase

Michihiro Suga,[a]‡ Naomine Yano,[b]‡ Kazumasa Muramoto,[b] Kyoko Shinzawa-Itoh,[b] Tomoko Maeda,[b] Eiki Yamashita,[a] Tomitake Tsukihara[a,b] and Shinya Yoshikawa[b]*

[a]Institute for Protein Research, Osaka University, 3-2 Yamada-oka, Suita, Osaka 565-0871, Japan, and [b]Department of Life Science, University of Hyogo, 3-2-1 Kouto, Kamighori, Akoh, Hyogo 678-1297, Japan

‡ These authors contributed equally to this work.

Correspondence e-mail: yoshi@sci.u-hyogo.ac.jp

Received 7 April 2011
Accepted 13 June 2011

PDB References: cytochrome *c* oxidase, 3asn; 3aso.

Fully oxidized cytochrome *c* oxidase (CcO) under enzymatic turnover is capable of pumping protons, while fully oxidized CcO as isolated is not able to do so upon one-electron reduction. The functional difference is expected to be a consequence of structural differences: [Fe^{3+}–OH^-] under enzymatic turnover *versus* [Fe^{3+}–O_2^{2-}–Cu^{2+}] for the as-isolated CcO. However, the electron density for O_2^{2-} is equally assignable to Cl^-. An anomalous dispersion analysis was performed in order to conclusively demonstrate the absence of Cl^- between the Fe^{3+} and Cu^{2+}. Thus, the peroxide moiety receives electron equivalents from cytochrome *c* without affecting the oxidation states of the metal sites. The metal-site reduction is coupled to the proton pump.

Cytochrome *c* oxidase (CcO) reduces molecular oxygen (O_2) to water (H_2O) in its O_2-reduction site, which includes two redox-active metal ions: Fe_{a3} (or haem a_3) and Cu_B. The reaction uses four electron equivalents obtained from cytochrome *c* *via* two metal sites, Cu_A and Fe_a (or haem *a*), in a reaction which is coupled to a proton-pumping process (Ferguson-Miller & Babcock, 1996). The mechanism of coupling the proton-pumping process to the electron-transfer reaction is one of the most important issues yet to be solved in the field of bioenergetics.

Under turnover conditions, Fe_{a3} in the O_2-reduction site receives O_2 when both metals are in the reduced state (R). The bound O_2 takes up four electrons (two of them from Fe_{a3}^{2+}, one from Cu_B^{1+} and one from a nearby tyrosine OH group) to break the O=O bond and provide the P intermediate, which has $Fe_{a3}^{4+}{=}O^{2-}$, $Cu_B^{2+}{-}OH^-$ and possibly a tyrosine radical in the O_2-reduction site. Four electron equivalents are then transferred from cytochrome *c* one at a time to the P intermediate, giving sequentially the F intermediate (a one-electron reduced state of P), the O intermediate (the fully oxidized state under turnover; 'turnover-oxidized state'), the E intermediate (a one-electron reduced state of O) and the R intermediate (Fe_{a3}^{2+}, Cu_B^{1+}, as described above). Each of the four electron-transfer steps from cytochrome *c* to CcO in each catalytic cycle is coupled to the pumping of a single proton equivalent (Bloch *et al.*, 2004). All of the four redox-active metal sites of CcO purified from beef heart under aerobic conditions are in the oxidized state as a result of the absence of an electron supply. The fully oxidized CcO is known as 'resting-oxidized CcO'. It does not pump protons upon addition of the initial two electron equivalents one at a time, in contrast to the case of the initial two-electron reduction of turnover-oxidized CcO, which drives the proton pump as described above (Bloch *et al.*, 2004).

The X-ray structure of resting-oxidized CcO suggests that a peroxide moiety bridges between Fe_{a3}^{3+} and Cu_B^{2+}. The O—O distance of 1.7 Å is significantly longer than the analogous O—O bond distance of typical model compounds (1.55 Å). This suggests that the bound peroxide is in an activated state (Aoyama *et al.*, 2009). However, resting-oxidized CcO is quite stable and its crystals can be stored at 277 K for several months without any significant absorption spectral change. Recently, a resonance Raman band assignable to the O—O stretching band of peroxide at 755 cm^{-1} has been reported for resting-oxidized CcO (Sakaguchi *et al.*, 2010). The band position

Table 1
Data-collection and refinement statistics.

	Data set 1†	Data set 2†	Data set 3
Data-collection statistics			
No. of crystals	4	1	1
Oscillation range (°)	0.75	0.50	0.75
No. of images	522 × 2	270	126 × 2
Space group	$P2_12_12_1$	$P2_12_12_1$	$P2_12_12_1$
Unit-cell parameters (Å)	a = 181.8, b = 204.1, c = 177.8	a = 182.0, b = 204.3, c = 177.9	a = 181.8, b = 204.2, c = 177.9
Wavelength (Å)	1.7470	0.9000	1.7470
Resolution (Å)	200–3.00 (3.03–3.00)	200–2.30 (2.33–2.30)	200–3.00 (3.03–3.00)
Observed reflections	4186814	1593006	1017322
Independent reflections	132667 (4364)	286689 (9457)	132242 (4360)
Averaged multiplicity‡	31.6 (31.2)	5.6 (5.5)	7.7 (7.5)
$\langle I/\sigma(I)\rangle$§	73.3 (46.0)	17.8 (4.5)	33.6 (18.5)
Completeness¶ (%)	100.0 (100.0)	99.9 (99.9)	99.7 (99.9)
$R_{\rm merge}$†† (%)	10.9 (17.8)	9.2 (46.3)	10.2 (17.3)
$R_{\rm p.i.m.}$ (%)	2.2 (3.3)		3.8 (6.5)
Refinement statistics			
R‡‡/$R_{\rm free}$§§ (%)	15.0/19.5	16.9/20.5	15.1/19.7
R.m.s.d.¶¶ bonds (Å)	0.022	0.025	0.022
R.m.s.d.¶¶ angles (°)	2.08	2.01	2.07

† The PDB entries for data sets 1 and 2 are 3asn and 3aso, respectively. ‡ Multiplicity is the number of observed reflections for each independent reflection. § $\langle I/\sigma(I)\rangle$ is the averaged intensity of the signal-to-noise ratio. ¶ Completeness is the percentage of independent reflections observed. †† $R_{\rm merge} = \sum_{hkl}\sum_i |I_i(hkl) - \langle I(hkl)\rangle| / \sum_{hkl}\sum_i I_i(hkl)$, where $I_i(hkl)$ is the intensity value of the ith measurement of hkl and $\langle I(hkl)\rangle$ is the corresponding mean value of $I(hkl)$ for all i measurements. The summation is over the reflections with $I/\sigma(I)$ larger than −3.0. ‡‡ R is the conventional crystallographic R factor, $\sum_{hkl} ||F_{\rm obs}| - |F_{\rm calc}|| / \sum_{hkl} |F_{\rm obs}|$, where $F_{\rm obs}$ and $F_{\rm calc}$ are the observed and calculated structure factors, respectively. §§ $R_{\rm free}$ is a free R factor evaluated for the 5% of reflections that are excluded from the refinement. ¶¶ R.m.s.d., root-mean-square deviation.

suggests an O—O bond distance of 1.5 Å. This is significantly shorter than the distance indicated in the X-ray structure. The resonance Raman band could arise from a minor species among multiple ligand species contributing to the electron density between the two metal ions in the O_2-reduction site. Therefore, quantitative evaluation of the occupancy of the peroxide which is responsible for the band at 755 cm^{-1} is not practical. It has been shown that six electron equivalents are required for complete reduction of resting-oxidized CcO (Mochizuki *et al.*, 1999). Although consistent with the peroxide-bound structure of the O_2-reduction site, these reductive titration results are not able to identify the structure of the electron acceptors in CcO. All of the X-ray, resonance Raman and reductive titration results provide strong but inconclusive evidence that a peroxide moiety bridges the two metal sites in the O_2-reduction site.

On the other hand, it has been shown that bovine heart CcO isolated in the presence of Cl^- by the method of Soulimane & Buse (1995) contains a tightly bound Cl^- ion in the O_2-reduction site (Fabian *et al.*, 2001). Thus, we cannot exclude the possibility that the bovine heart CcO preparation used for the X-ray structural analysis described above contains a Cl^- ion at the O_2-reduction site even though the enzyme was isolated in the absence of Cl^- from the reagents used during purification (Mochizuki *et al.*, 1999). Furthermore, one equivalent of Cl^- equally distributed between the two sites (Cu_B and Fe_{a3}) would provide electron density which is essentially identical to the electron density provided by one equivalent of peroxide bridged between the two metal ions. If Cl^- was present in the O_2-reduction site it would be unlikely to receive electrons from either of the two metals. Thus, a Cl^--bound form would be expected to be very stable. This is consistent with the stability of the resting-oxidized CcO (Aoyama *et al.*, 2009). X-ray crystallographic analysis has been performed for *Paracoccus denitrificans* CcO treated with excess bromide ion, which would displace the Cl^- at the O_2-reduction site and provide bromide-based anomalous dispersion signals (Koepke *et al.*, 2009). However, no Bijvoet difference electron density at the O_2-reduction site was detected for *P. denitrificans* CcO treated with bromide (Koepke *et al.*, 2009). The O_2-reduction site may have much weaker affinity for bromide than chloride and thus the absence of bromide does not necessarily prove the absence of chloride in the O_2-reduction site. Although the electron density in the O_2-reduction site is fully consistent with a chloride-bound structure, no conclusive evidence for chloride binding to the O_2-reduction site has been reported.

Convincing structural information regarding the O_2-reduction site of resting-oxidized CcO would provide various insights into the proton-pumping mechanism. Furthermore, the mechanism of proton decoupling induced by a chloride ion at the O_2-reduction site would vary significantly from the mechanism induced by a peroxide moiety. For direct elemental analysis of the O_2-reduction site, the difference anomalous electron density between Fe_{a3} and Cu_B was examined for the resting-oxidized form of bovine heart CcO using 1.7470 Å wavelength X-ray beams, which provide a slightly larger anomalous scattering factor of $\Delta f'' = 0.89$ for Cl compared with Fe ($\Delta f'' = 0.47$), Cu ($\Delta f'' = 0.74$) and S ($\Delta f'' = 0.70$).

An X-ray diffraction data set was collected at 50 K at an X-ray wavelength of 1.7470 Å to 3.0 Å resolution with a high redundancy of 31.4 in the highest resolution shell in order to increase the accuracy of determination of the electron density (Table 1). The irradiation period was minimized by changing the irradiation position after each set of 40 irradiations, using four large crystals (500 × 500 × 200 µm) for the full data-set collection with an X-ray beam of size 50 × 50 µm (data set 1). The diffraction images were collected using the inverse-beam mode in order to reduce the effect of X-ray damage on the Bijvoet differences. In addition to data set 1, an X-ray data set (data set 2) was collected at an X-ray wavelength of 0.9 Å to 2.3 Å resolution using a crystal isomorphous to that used to obtain data set 1. Data set 2 was used for phase determination and structural refinement.

The phases of data set 2 were initially determined by rigid-body refinement at 4.0 Å resolution using the CcO model previously determined at 1.8 Å resolution (PDB entry 2dyr; Shinzawa-Itoh *et al.*, 2007) and then by restrained refinement at 2.3 Å resolution. The refinement converged well to an R value of 0.169 and an $R_{\rm free}$ of 0.205. The phases of data set 1 were determined at 3.0 Å resolution by restrained refinement using the structure obtained from data set 2. The refinement converged well to an R value of 0.150 and an $R_{\rm free}$ value of 0.195.

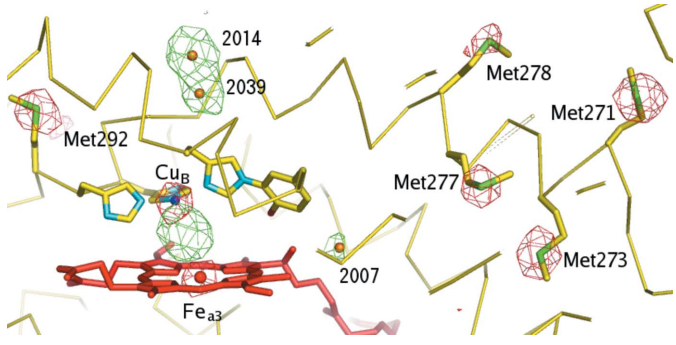

Figure 1
($F_o - F_c$) difference electron-density and Bijvoet difference Fourier maps for the O_2-reduction site: green cages denote the ($F_o - F_c$) difference electron-density map between the Fe_{a3}–Cu_B site and the three water molecules near the metal site contoured at the 3.5σ level (1σ = 0.0218 e^- $Å^{-3}$). The red cages denote the Bijvoet difference Fourier map contoured at the 4.0σ level (1σ = 0.00543 e^- $Å^{-3}$). The model shows the structure obtained using data set 2.

Table 2
Anomalous peaks.

Anomalous peak site	Peak height (σ level)	
	Data set 1	Data set 3
Cu_B	9.5	4.0
Fe_{a3}	8.0	3.1
Fe_a	7.8	4.3
S^{δ} (Met271)	11.9	6.7
S^{δ} (Met273)	10.9	7.4
S^{δ} (Met277)	7.9	4.5
S^{δ} (Met278)	5.8	3.8
S^{δ} (Met292)	8.7	5.1
S (averaged)†	8.4	4.4
1σ (e^{-} Å^{-3})	0.00478	0.00986

† Of the 34 S atoms in subunit I, Met1, for which the electron density is weak, was excluded from evaluation of the averaged peak height of S atoms.

Fig. 1 shows ($F_o - F_c$) difference electron-density and Bijvoet difference Fourier maps for the O_2-reduction site, including seven methionine residues near the O_2-reduction site, calculated from data set 1 at 3.0 Å resolution. The maps are depicted together with structural models of haem a_3, Cu_B and three water molecules (2007, 2014 and 2039 in Fig. 1) that are always observed in the CcO crystal structure. In the ($F_o - F_c$) map calculation three water molecules were excluded from the refinement. The ($F_o - F_c$) peak height between Fe_{a3} and Cu_B was 2.0 times higher than the averaged peak height for the three reference water molecules, which is consistent with previous results (Aoyama *et al.*, 2009). Thus, under the present X-ray diffraction experimental conditions no significant decrease in the electron density owing to hydrated electrons, as observed in the X-ray diffraction experiments at 100 K using 0.9 Å X-rays, was identified between Fe_{a3} and Cu_B in spite of the use of longer wavelength X-rays.

Bijvoet difference maps were calculated for data sets 1 and 3, both of which were obtained at 3.0 Å resolution (Tables 1 and 2). Data set 3, which consists of part of data set 1, was used to examine the effect of the multiplicity on the signal-to-noise ratio of the anomalous density. The significant anomalous density expected for a Cl atom was not detected between Fe_{a3} and Cu_B, in spite of the larger anomalous scattering factor, $\Delta f''$, of the Cl atom at this X-ray wavelength relative to those of Fe, Cu and S atoms. In the Bijvoet difference map from the highly redundant data set 1, Cu_B, Fe_{a3} and Fe_a were identified as isolated peaks of 9.5σ, 8.0σ and 7.8σ, respectively (Table 2). The peaks are significantly clearer than those from data set 3. Of the 34 S atoms in subunit I, 33 atoms were identified in the peaks with an average height of 8.4σ. Consequently, the Bijvoet difference map clearly indicates that a Cl atom is not located between Fe_{a3} and Cu_B. No peaks corresponding to a chloride ion were detected in any other site within the unit cell.

These results are consistent with the quantitative analysis for chloride content of crystalline bovine heart CcO in the resting-oxidized form. The chloride content in the crystalline preparation was determined using an ion-chromatogram system (Dionex ICS-2000) after heat treatment of the crystalline sample at 1373 K. 65 nmol of crystalline enzyme (13 mg protein) was used in each determination. Duplicate determinations were performed for each enzyme preparation. The averaged value for three different preparations was 0.15 ($\pm$ 0.03) moles of chloride per mole of CcO. This method is presently the most direct and reliable for chloride analysis, although fairly large amounts of protein are required.

The present results negate the possibility that chloride is bound at the O_2-reduction site. The O—O bond length of 1.7 Å is significantly longer than those of typical peroxide compounds. This is not consistent with the stability of the resting-oxidized CcO as described above. It is desirable to improve the resolution of the X-ray structure in order to identify the structural basis for the stability of resting-oxidized CcO. A possible physiological role of the resting-oxidized CcO is to prevent the formation of reactive oxygen species by transition metals in the O_2-reduction site under a low rate of electron flow from upstream of the respiratory chain.

Turnover-oxidized CcO has OH^- bound to Fe^{3+}_{a3} as demonstrated by resonance Raman analyses (Ogura *et al.*, 1996), in contrast to the bridging peroxide that is observed between Fe^{3+}_{a3} and Cu^{2+}_B in resting-oxidized CcO. Upon the donation of each of the initial two electron equivalents to turnover-oxidized CcO the process of proton pumping begins. In contrast, resting-oxidized CcO (with bridging peroxide) does not pump protons under the same conditions (Bloch *et al.*, 2004). When the initial two electron equivalents are provided to the latter, the enzyme is expected to reduce the bridging peroxide completely to the oxide level ($2O^{2-}$) without affecting the oxidation states of the two metal sites. A lag phase detectable in the reductive titration curve for resting-oxidized CcO supports the initial two-electron donation to resting-oxidized CcO without reducing the two metal sites in the O_2-reduction site (Mochizuki *et al.*, 1999). On the other hand, when the initial two electron equivalents are provided to turnover-oxidized CcO they are used for reduction of the two metal ions in the O_2-reduction site. Thus, the bound peroxide decouples the proton pump by trapping the electron equivalents to avoid reduction of the two metals. Reduction of haem a_3 or Cu_B is expected to trigger the proton pump driven by haem a, which is located close to these metal sites. X-ray structural characterization of turnover-oxidized CcO at high resolution is expected to provide a more concrete structural basis for the coupling mechanism.

This work was supported in part by Grant-in-Aids for Scientific Research on Priority Areas 16087206 (TT), 16087208 and 222247012 (SY), the Targeted Protein Research Program (KM, KS-I and SY) and the Global Center of Excellence Program (SY) all provided by the Japanese Ministry of Education, Culture, Sports, Science and Technology. SY is a Senior Visiting Scientist of the RIKEN Harima Institute.

References

Aoyama, H., Muramoto, K., Shinzawa-Itoh, K., Hirata, K., Yamashita, E., Tsukihara, T., Ogura, T. & Yoshikawa, S. (2009). *Proc. Natl Acad. Sci. USA*, **106**, 2165–2169.
Bloch, D., Belevich, I., Jasaitis, A., Ribacka, C., Puustinen, A., Verkhovsky, M. I. & Wikström, M. (2004). *Proc. Natl Acad. Sci. USA*, **101**, 529–533.
Fabian, M., Skultety, L., Brunel, C. & Palmer, G. (2001). *Biochemistry*, **40**, 6061–6069.
Ferguson-Miller, S. & Babcock, G. T. (1996). *Chem. Rev.* **96**, 2889–2908.
Koepke, J., Olkhova, E., Angerer, H., Müller, H., Peng, G. & Michel, H. (2009). *Biochim. Biophys. Acta*, **1787**, 635–645.
Mochizuki, M., Aoyama, H., Shinzawa-Itoh, K., Usui, T., Tsukihara, T. & Yoshikawa, S. (1999). *J. Biol. Chem.* **274**, 33403–33411.
Ogura, T., Hirota, S., Proshlyakov, D. A., Shinzawa-Itoh, K., Yoshikawa, S. & Kitagawa, T. (1996). *J. Am. Chem. Soc.* **118**, 5443–5449.
Sakaguchi, M., Shinzawa-Itoh, K., Yoshikawa, S. & Ogura, T. (2010). *J. Bioeneng. Biomembr.* **42**, 241–243.
Shinzawa-Itoh, K., Aoyama, H., Muramoto, K., Terada, H., Kurauchi, T., Tadehara, Y., Yamasaki, A., Sugimura, T., Kurono, S., Tsujimoto, K., Mizushima, T., Yamashita, E., Tsukihara, T. & Yoshikawa, S. (2007). *EMBO J.* **26**, 1713–1725.
Soulimane, T. & Buse, G. (1995). *Eur. J. Biochem.* **227**, 588–595.